Article

Alkali-Added Catalysts Based on LaAlO$_3$ Perovskite for the Oxidative Coupling of Methane

Suna An, JeongHyun Cho, Dahye Kwon and Ji Chul Jung *

Department of Chemical Engineering, Myongji University, Yongin 17058, Korea; suna960312@gmail.com (S.A.);
po78jhjh@gmail.com (J.C.); kdahye829@gmail.com (D.K.)
* Correspondence: jcjung@mju.ac.kr

Abstract: In this study, we aimed to enhance the catalytic activity of perovskite catalysts and elucidate their catalytic behavior in the oxidative coupling of methane (OCM), using alkali-added LaAlO$_3$ perovskite catalysts. We prepared LaAlO$_3$_XY (X = Li, Na, K, Y = mol %) catalysts and applied them to the OCM reaction. The results showed that the alkali-added catalysts' activities were promoted compared to the LaAlO$_3$ catalyst. In this reaction, ethane was first synthesized through the dimerization of methyl radicals, which were produced from the reaction of methane and oxygen vacancy in the perovskite catalysts. The high ethylene selectivity of the alkali-added catalysts originated from their abundance of electrophilic lattice oxygen species, facilitating the selective formation of C$_2$ hydrocarbons from ethane. The high CO$_x$ (carbon monoxide and carbon dioxide) selectivity of the LaAlO$_3$ catalyst originated from its abundance of nucleophilic lattice oxygen species, favoring the selective production of CO$_x$ from ethane. We concluded that electrophilic lattice oxygen species play a significant role in producing ethylene. We obtained that alkali-adding could be an effective method for improving the catalytic activity of perovskite catalysts in the OCM reaction.

Keywords: oxidative coupling of methane; perovskites; LaAlO$_3$; alkali metals; electrophilic lattice oxygen

1. Introduction

Since the industrial revolution of the late 18th century, total oil consumption has been increasing gradually with the industrial development of developing countries. Oil depletion is expected to accelerate under these circumstances. Shale gas has attracted significant attention as an upcoming alternative energy source. It has significant reserves in the world, and about 80% to 90% of its components consist of methane (CH$_4$). As shale gas is drawing attention as an alternative energy source, the study of converting methane, which is the main component of shale gas, into high value-added compounds is being actively conducted [1–5].

CH$_4$ has enormous potential as a feedstock for various valuable chemicals and fuel production. There are two methods of converting CH$_4$ into high value-added compounds: direct conversion and indirect conversion of CH$_4$. The indirect conversion of CH$_4$ requires additional energy because it needs a multi-step process [6–9]. For this reason, many researchers believe that the direct conversion of CH$_4$ is more efficient in economic terms [10–13]. Among the direct CH$_4$ conversion methods, the oxidative coupling of methane (OCM) to form C$_2$ hydrocarbons such as ethylene (C$_2$H$_4$) and ethane (C$_2$H$_6$) has recently attracted attention [14–19]. It has been studied since the 1980s, but it has not been commercialized for various reasons until now. Representative reasons are that a high reaction temperature is required and that a complete oxidation reaction of CH$_4$ occurs competitively. Therefore, it is essential to develop a catalyst capable of lowering the reaction temperature or of promoting partial oxidation of CH$_4$ [20–23].

Many researchers have conducted studies to identify the active site of the catalyst with high catalytic activities in the OCM to overcome this problem. According to previous

reports on the OCM, the $Na_2/WO_4/Mn/SiO_2$ catalyst is considered the best catalyst for the OCM reaction [24–28]. Nevertheless, there remains a great deal of ambiguity concerning the nature and properties of the active sites because of their complex composition and structure [29].

There are many studies on catalysts for the OCM with a simpler structure than Na/W/Mn metal oxide catalysts [21,22]. The most classically used catalyst is the MgO catalyst, which is an alkaline earth oxide catalyst. However, this catalyst is reported to show a low C_2 yield of about 5% to 7% at 800 °C [30]. Research on catalysts in which alkali metals such as Li are doped into alkaline earth metal catalysts to overcome the drawbacks of low reaction activity has been reported [31–33]. For the MgO catalyst to which Li was added, the C_2 yield increased by about 10% compared to the MgO catalyst. Therefore, many researchers have tried to improve the OCM catalytic activity using various additives. Among them, the most typical additive is alkali metal, and many studies have reported that it was added to promote the OCM catalytic activity [34–37]. Rane et al. [38] reported that the C_2 selectivity of CaO catalyst increased by adding alkali metals to the catalyst. Malekzadeh et al. [39] reported that the alkali metals were added to the $(Mn + W)/SiO_2$ catalyst to enhance the catalytic activity. However, it is still relatively low to commercialize the OCM.

Meanwhile, the $LaAlO_3$ perovskite catalyst is reported to have a simple structure and high thermal stability. Besides, it shows considerable catalytic activities in the OCM reaction and can be easily produced by various methods [40,41]. Thus, the $LaAlO_3$ perovskite catalyst can be considered as a good model catalyst to investigate the active site in the OCM. We aimed to improve the catalyst activities by adding alkali metals to the $LaAlO_3$ perovskite catalysts and to demonstrate their catalytic behavior in the OCM reaction.

2. Materials and Methods

2.1. Catalyst Preparation

$LaAlO_3\_XY$ (X = Li, Na, K, Y = mol %) catalysts were prepared using a citrate sol-gel method. Lanthanum nitrate ($La(NO_3)_3 \cdot 6H_2O$, Sigma Aldrich, St. Louis, MO, USA), aluminum nitrate ($Al(NO_3)_3 \cdot 9H_2O$, Sigma Aldrich), and alkali metals (lithium nitrate ($LiNO_3$), sodium nitrate ($NaNO_3$), potassium nitrate (KNO_3) (Sigma Aldrich), were employed as metal precursors. 0.00625 mol of $La(NO_3)_3$ precursor was dissolved in 25 mL of deionized water (solution A). 0.00625 mol of $Al(NO_3)_3$ was dissolved in 25 mL of deionized water (solution B). 5 mol % of alkali metals and 0.02632 mol of citric acid were dissolved in 100 mL deionized water (solution C). Solutions A and B were added dropwise into solution C upon stirring at 600 rpm. After stirring the mixed solution at room temperature for 1 h, the water was evaporated at 80 °C until a gel was obtained, which was then dried overnight in a convection oven at 200 °C. After grinding the dried gel using a mortar, $LaAlO_3\_XY$ (X = Li, Na, K, Y = mol %) catalysts were finally obtained by calcination in a muffle furnace at 950 °C for 5 h.

2.2. Catalyst Characterization

The crystalline structures of the prepared $LaAlO_3\_XY$ (X = Li, Na, K, Y = mol %) catalysts were confirmed by powder X-ray diffraction (XRD) measurements using X'pert-Pro PAN-analytical diffractometer with Cu-Kα radiation (λ = 1.54056 Å). The diffraction patterns were recorded within the 2θ range: 10° to 90°. To confirm the specific surface area of the prepared catalysts, nitrogen adsorption–desorption isotherms were determined using a constant-volume adsorption apparatus (TriStar II 3020, Micromeritics) at −196 °C. The specific surface area was determined using the Brunauer–Emmett–Teller (BET) equation. Inductively coupled plasma atomic emission spectroscopy (ICP-AES) analysis was conducted using an ICPS-8100 spectrometer (Shimadzu) to confirm the chemical composition of the catalysts. The field emission scanning electron microscope (FE-SEM) images were obtained on an EM-30AX (COXEM). The prepared catalysts were pretreated by conducting resin and coating with platinum. X-ray photoelectron spectroscopy (XPS) analysis was

conducted using a K-alpha instrument (Thermo Fisher) equipped with a monochromatic Al Kα X-ray source to determine the O 1s binding energies of the catalysts, which were calibrated based on the C 1s peak at 284.5 eV. CO_2-temperature-programmed desorption (CO_2-TPD) measurement was conducted using a BELCAT B (MicrotracBEL, Osaka, Japan) and each catalyst (0.05 g) was loaded into the quartz reactor for the TPD apparatus. It was pretreated at 400 °C for 1 h under a flow of He (30 mL/min). Once cooled down to room temperature with helium, 5% CO_2 in He (30 mL/min) was pulsed into the reactor at room temperature for 40 min to adsorb CO_2. Finally, it was purged at room temperature with He for 30 min to desorb physically adsorbed CO_2. The CO_2-TPD profiles of the catalysts were recorded from room temperature to 950 °C at a heating rate of 10 °C/min and the desorbed CO_2 was detected by a thermal conductivity detector (TCD).

2.3. Catalytic Reaction

The OCM was conducted via a continuous flow quartz reactor with an internal diameter of 6 mm. The catalyst was loaded on the reactor by closing the upper and lower ends of the catalysts with quartz wool. The empty space of the reactor was filled with zirconia–silica ceramic beads. The reactor was heated to 775 °C under nitrogen flow, and the feed was then changed to the reactant feed (CH_4:O_2:N_2 = 3:1:1, *v/v/v*). The total reactant volume flow rate was fixed at 20 mL/min with a gas hourly space velocity of 10,000 h^{-1}. A cold trap was employed to remove the water vapor produced during the reaction. An on-line gas chromatography system (YL-6500, Younglin, Korea) with a flame ionization detector (FID) and a thermal conductivity detector (TCD) was conducted to periodically analyze gas products. A carboxen-1000 column was used to separate the reaction products. CH_4 and C_2 hydrocarbons were detected by the FID, while CO and CO_2 were detected by the TCD. The catalytic performance of CH_4 conversion and C_2 and CO_x selectivity were calculated using the following equations. The yield of C_2 hydrocarbons was obtained by multiplying the value obtained for methane conversion with that of C_2 selectivity.

$$CH_4 \text{ conversion } (\%) = \frac{\text{moles of } CH_4 \text{ consumed}}{\text{moles of } CH_4 \text{ in the feed}} \times 100$$

$$C_2 \text{ Selectivity } (\%) = \frac{2 \times \text{moles of } C_2 \text{ hydrocarbons in the output stream}}{\text{moles of } CH_4 \text{ in the feed}} \times 100$$

$$CO_X \text{ Selectivity } (\%) = \frac{\text{moles of } CO_X \text{ in the output stream}}{\text{moles of } CH_4 \text{ in the feed}} \times 100$$

3. Results and Discussion

3.1. Formation of LaAlO$_3$_XY (X = Li, Na, K, Y = mol %) Catalysts

LaAlO$_3$ catalysts are generally reported to have excellent thermal stability and considerable activity in the OCM. In this study, we prepared LaAlO$_3$_XY (X = Li, Na, K, Y = mol %) catalysts by adding alkali metals to the LaAlO$_3$ catalyst to increase the catalytic activity. The LaAlO$_3$ catalyst was prepared in the same method for comparison.

We performed powder XRD measurements to confirm the structural properties of LaAlO$_3$_XY and LaAlO3 catalysts. A JCPDS card (LaAlO$_3$: #85-0848) was used to confirm all the XRD peaks [40]. As shown in Figure 1, only XRD peaks for the LaAlO$_3$ perovskite were found in LaAlO$_3$_X5, LaAlO$_3$_X10, and LaAlO$_3$_X20 catalysts. It showed that LaAlO$_3$_X5, LaAlO$_3$_X10, and LaAlO$_3$_X20 catalysts have been successfully prepared. However, LaAlO$_3$_X30 catalyst showed other peaks with the LaAlO$_3$ perovskite peak. Thus, we conducted an OCM reaction using LaAlO$_3$_X5, LaAlO$_3$_X10, LaAlO$_3$_20 catalysts, excluding the LaAlO$_3$_X30 catalyst.
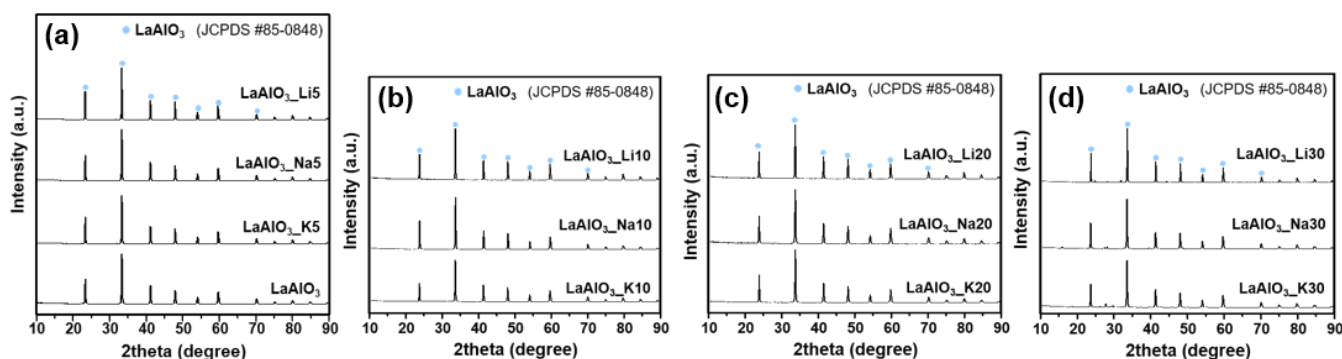
Figure 1. X-ray diffraction (XRD) patterns of the prepared LaAlO$_3$_XY (X = Li, Na, K, Y = mol %) and LaAlO$_3$ catalysts: (**a**) LaAlO$_3$_X5, (**b**) LaAlO$_3$_X10, (**c**) LaAlO$_3$_X20, and (**d**) LaAlO$_3$_X30.

3.2. Catalyst Performance of LaAlO$_3$_XY (X = Li, Na, K, Y = mol %) Catalysts in the OCM

The prepared LaAlO$_3$_XY (X = Li, Na, K, Y = mol %) catalysts were applied to the OCM reaction. Figure 2 shows the obtained results of the catalyst activities. For comparison, the catalytic activity of the LaAlO$_3$ catalyst was shown in Figure 2. The reaction was conducted three times to show the average value of the catalytic activities. The standard deviation of the experimental values was shown by the red line. Interestingly, C$_2$ yield and selectivity increased as the content on the added alkali metal increased. All LaAlO$_3$_XY catalysts presented higher C$_2$ yield and selectivity than the LaAlO$_3$ catalyst. Among them, LaAlO$_3$_Li20 catalyst showed the highest C$_2$ yield. In particular, the ratio of CO and CO$_2$ varied greatly depending on the prepared catalysts. Alkali metal-added LaAlO$_3$_XY catalyst showed higher CO$_2$ selectivity than the LaAlO$_3$ catalyst.
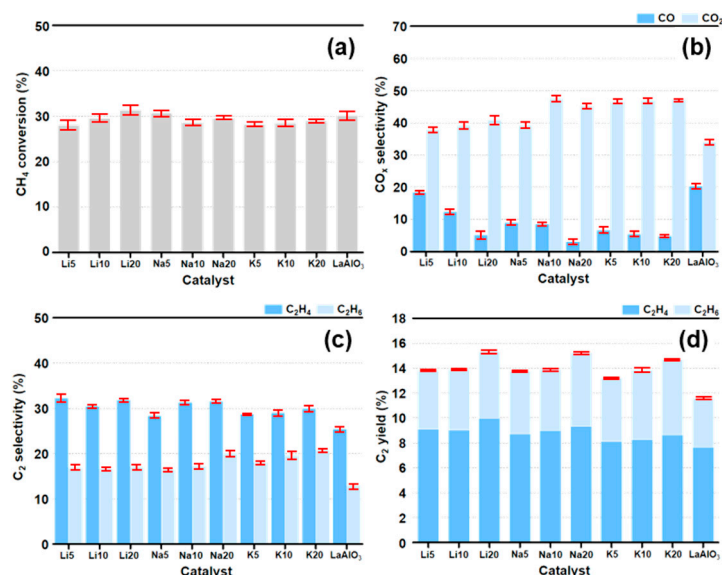

Figure 2. Catalytic activities in terms of the prepared catalyst in the oxidative coupling of methane (OCM): (**a**) CH$_4$ conversion (%), (**b**) CO$_x$ selectivity (%), (**c**) C$_2$ selectivity (%), and (**d**) C$_2$ yield (%).

From these results, it was confirmed that LaAlO$_3$_XY and LaAlO$_3$ catalysts have the same perovskite structure but that they showed different catalytic activities. Additionally, it was confirmed that the catalytic activity can be promoted by adding alkali metals to the LaAlO$_3$ catalyst. We obtained that, among LaAlO$_3$_XY catalysts with increased activity, LaAlO$_3$_X5, which had the effect of increasing activity with the smallest amount of alkali metal added, was the most meaningful. We tried to investigate the active site of the catalyst for the OCM using LaAlO$_3$_X5 catalysts.

3.3. Catalyst Performance of LaAlO₃_X5 (X = Li, Na, K) Catalysts in the OCM

Figure 3 shows the results of the catalytic activities for the OCM reaction using LaAlO$_3$_X5 (X = Li, Na, K) catalysts. Figure 3 shows the LaAlO$_3$ catalyst's results for comparison. The reaction was performed three times, as in the previous experiment, showing an average value of the activity. The standard deviation of the experimental values is shown by the red line. In the catalytic activities' results, the CH$_4$ conversion of LaAlO$_3$_X5 and LaAlO$_3$ catalysts was about 30% for all four catalysts. However, the C$_2$ selectivity, Cox selectivity, and C$_2$ yield of prepared catalysts were considerably different. For C$_2$ selectivity, LaAlO$_3$_Li5, LaAlO$_3$_K5, LaAlO$_3$_Na5, and LaAlO$_3$ were higher (in that order). LaAlO$_3$_X5 catalysts increased by about 8% compared to the LaAlO$_3$ catalyst. In C$_2$ yield's results, LaAlO$_3$_Li5, LaAlO$_3$_Na5, LaAlO$_3$_K5, and LaAlO$_3$ were the highest (in that order). In general, LaAlO$_3$_X5 catalysts increased by about 2% compared to the LaAlO$_3$ catalyst. The CO selectivity and the CO$_2$ selectivity of the four catalysts were also considerably different. The CO selectivity increased in the order of LaAlO$_3$, LaAlO$_3$_Li5, LaAlO$_3$_Na5, and LaAlO$_3$_K5. The CO$_2$ selectivity was higher in the order of LaAlO$_3$_K5, LaAlO$_3$_Na5, LaAlO$_3$_Li5, and LaAlO$_3$. The prepared catalysts showed considerably different catalytic activities. Therefore, we analyzed the causes of these differences in activities and investigated the active sites of the catalysts for the OCM in this study.
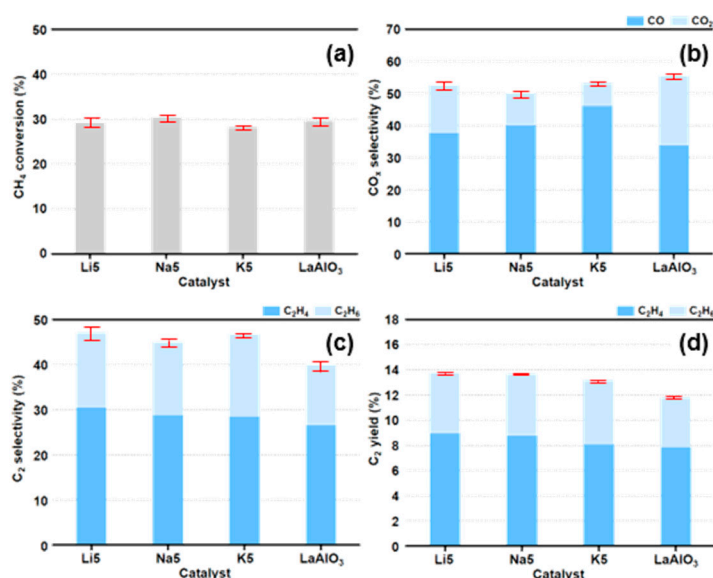

Figure 3. Catalytic activities in terms of LaAlO$_3$_X5 and LaAlO$_3$ catalysts in the OCM: (**a**) CH$_4$ conversion (%), (**b**) CO$_x$ selectivity (%), (**c**) C$_2$ selectivity (%), and (**d**) C$_2$ yield (%).

3.4. Physical Properties and Chemical Composition of LaAlO₃_X5 (X = Li, Na, K) Catalysts

Although LaAlO$_3$_X5 (X = Li, Na, K) catalysts and the LaAlO$_3$ catalyst had the same LaAlO$_3$ perovskite structure, the catalytic activities were considerably different for the OCM. We performed BET, ICP-AES, and FE-SEM analysis to confirm the physical and chemical properties of the prepared catalysts prior to investigating the active site of the catalysts.

We performed BET analysis to compare the specific surface area of the catalysts used in the reaction. Table 1 contains the analysis results. From the BET analysis results, it was confirmed that LaAlO$_3$_X5 catalysts had reduced specific surface area compared to the LaAlO$_3$ catalyst. The specific surface area of the existing LaAlO$_3$ catalyst was 3.5 m^2/g, and the Li-added LaAlO$_3$_Li5 catalyst had the smallest specific surface area of 1.4 m^2/g. LaAlO$_3$_Na5 and LaAlO$_3$_K5 catalysts showed 2.9 and 3.1 m^2/g of specific surface area, respectively. These results were consistent with the results of many studies that the addition of alkali metals to conventional catalysts reduces the specific surface area of the catalyst. We confirmed that the catalysts' properties were influenced by adding alkali metals to the

$LaAlO_3$ catalyst through these results. Although the specific surface areas of the catalysts were reduced by adding alkali metals, the CH_4 conversions of $LaAlO_3$_X5 catalysts were similar to that of the $LaAlO_3$ catalyst. These results are not common in catalysis; according to the studies, it is expected that the methyl radical binding occurs in the weather after CH_4 is converted from the catalyst surface to methyl radicals [36].

Table 1. Specific surface of $LaAlO_3$_X5 (X = Li, Na, K) and $LaAlO_3$ catalysts.

Catalyst	S_{BET} (m^2/g) [a]
$LaAlO_3$_Li5	1.4
$LaAlO_3$_Na5	2.9
$LaAlO_3$_K5	3.1
$LaAlO_3$	3.5

[a] Specific surface area was calculated using the Brunauer–Emmett–Teller (BET) plot.

Table 2 shows the ICP-AES analysis results for $LaAlO_3$_X5 and $LaAlO_3$ catalysts. For the $LaAlO_3$_Li5 catalyst with the addition of Li, it was confirmed that all the Li added was volatilized during the calcination of the catalyst manufacturing process and did not remain. Li species evaporation is consistent with previous literature reports [42]. According to previous studies, Li species in Li-doped MgO catalysts were vaporized at about 760–860 K through the reaction of Li species with oxygen. Therefore, it was expected that Li species were volatilized during the calcination process. For $LaAlO_3$_Na5 and $LaAlO_3$_K5 catalysts with the addition of Na and K, it was confirmed that about 1 mol % of Na and K remained. Studies have confirmed that when alkali metals, such as Na and K, are added in perovskite catalysts, the amount remains less than the actual amount added since the ionic radii do not match [43].

Table 2. Chemical composition of $LaAlO_3$_X5 (X = Li, Na, K) catalysts.

Catalyst	La	Al	Li	Na	K
	mol %				
$LaAlO_3$_Li5	53.3	46.7	-	-	-
$LaAlO_3$_Na5	52.6	46.3	-	1.1	-
$LaAlO_3$_K5	52.8	46.5	-	-	0.7

We conducted an FE-SEM analysis on the alkali metal-added $LaAlO_3$_X5 and $LaAlO_3$ catalysts to confirm the surface changes of the catalysts. Figure 4 shows the results. The FE-SEM analysis result confirmed that the surface of the $LaAlO_3$_X5 catalysts with the alkali metal added and the existing $LaAlO_3$ catalyst were considerably different. For the $LaAlO_3$ catalyst, it was confirmed that the surface of the catalyst was relatively smooth. However, $LaAlO_3$_X5 catalysts showed relatively uneven surfaces. The catalyst surface of the $LaAlO_3$_Li5 catalyst was considerably different compared to the $LaAlO_3$ catalyst, even though there was no Li left in the catalyst. It was confirmed that Li was volatilized and that the structural change of the catalyst occurred. For $LaAlO_3$_Na5 and $LaAlO_3$_K5 catalysts, the addition of the added alkali metals caused a structural change in the $LaAlO_3$ catalyst, which was expected.
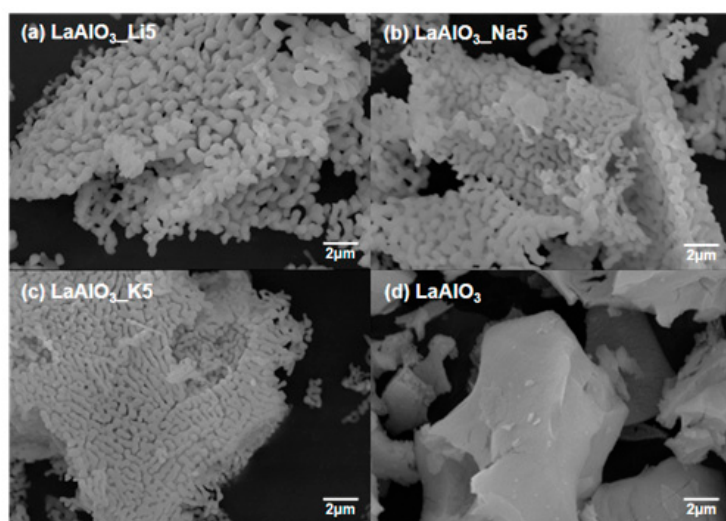
Figure 4. Field emission scanning electron microscopy images (FE-SEM) of $LaAlO_3\_X5$ (X = Li, Na, K) and $LaAlO_3$ catalysts: (**a**) $LaAlO_3\_Li5$, (**b**) $LaAlO_3\_Na5$, (**c**) $LaAlO_3\_K5$, and (**d**) $LaAlO_3$.

3.5. Investigation of the Active Site of $LaAlO_3\_X5$ (X = Li, Na, K) and $LaAlO_3$ Catalysts on the OCM

3.5.1. The Active Site of $LaAlO_3\_X5$ (X = Li, Na, K) and $LaAlO_3$ Catalysts for C_2 Selectivity and CO_x Selectivity

The three $LaAlO_3\_X5$ (X = Li, Na, K) and $LaAlO_3$ catalysts showed quite different catalytic activities for the OCM. From the difference in catalytic activities, it was confirmed that the correlation between the active site of the catalyst, particularly the oxygen species on the surface of the catalyst and the activity, can be properly investigated. The active site of the catalyst used in the OCM has not been understood. Heterogeneous and homogeneous reactions occur simultaneously in the OCM reaction. The activity of the catalytic reaction is quite related to the surface oxygen species properties of the catalysts, according to many studies on the OCM [44–48]. We conducted an XPS analysis for the prepared four catalysts to investigate the surface oxygen species properties of the catalysts.

XPS analysis for prepared the catalysts was performed, and the results are shown in Figure 5. The red line in the graph showed the nucleophilic lattice oxygen species ($O_{lat(n)}$), and the blue line showed the electrophilic lattice oxygen species ($O_{lat(e)}$). From these results, the relative areas and area ratios corresponding to the nucleophilic oxygen species ($O_{lat(n)}$) and the electrophilic oxygen species ($O_{lat(e)}$) of the catalytic lattice oxygen were calculated in Table 3. The $LaAlO_3\_X5$ catalysts to which the alkali metal was added possessed a relatively abundant electrophilic lattice oxygen species compared to the $LaAlO_3$ catalyst. The $LaAlO_3\_Li5$ catalyst with the highest C_2 selectivity had a relatively large amount of electrophilic lattice oxygen species ($O_{lat(e)}$). However, the $LaAlO_3$ catalyst with the lowest C_2 selectivity possessed the least electrophilic lattice oxygen species ($O_{lat(e)}$). For the nucleophilic oxygen species, it was confirmed that the oxygen species were abundant in the order of $LaAlO_3$, $LaAlO_3\_K5$, $LaAlO_3\_Li5$, and $LaAlO_3\_Na5$ catalysts. The $LaAlO_3$ catalyst with the highest CO_x selectivity had the relatively highest nucleophilic oxygen species, and the $LaAlO_3\_Na5$ catalyst with the lowest CO_x selectivity had the relatively lowest nucleophilic oxygen species. When these XPS analysis results were compared with the catalytic activities for the OCM, it was expected that the CH_4 adsorbed by the adsorbed oxygen species on the catalyst surface would be converted to the methyl radical from the catalyst surface [49,50]. After that, C_2H_6 was formed by the combination of two methyl radicals. Thus, we concluded that the electrophilic lattice oxygen species ($O_{lat(e)}$) on the catalyst surface were responsible for converting C_2H_6 into C_2H_4, and the nucleophilic lattice oxygen species ($O_{lat(e)}$) were responsible for converting C_2H_6 into CO or CO_2 according to the strength of the nucleophilic lattice oxygen species.
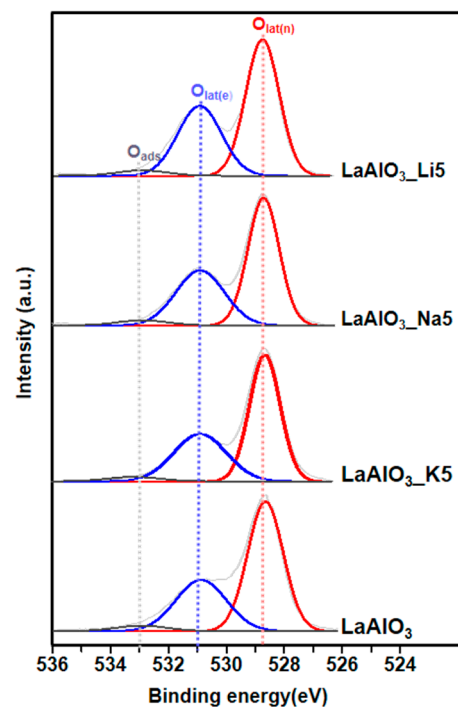
Figure 5. O 1s X-ray photoelectron spectroscopy (XPS) spectra of $LaAlO_3$_X5 (X = Li, Na, K) and $LaAlO_3$ catalysts.

Table 3. Curve-fitted and quantified O 1s XPS peaks for $LaAlO_3$_X5 (X = Li, Na, K) and $LaAlO_3$ catalysts.

Catalyst	Relative Amount (%)			$O_{lat(e)}/O_{lat(n)}$
	O_{ads} (533.0 eV)	$O_{lat(e)}$ (531.0 eV)	$O_{lat(n)}$ (528.8 eV)	
$LaAlO_3$_Li5	3.6	38.6	57.9	0.67
$LaAlO_3$_Na5	3.7	38.5	57.8	0.67
$LaAlO_3$_K5	3.5	37.7	58.8	0.64
$LaAlO_3$	3.7	34.6	61.7	0.56

3.5.2. The Active Site of $LaAlO_3$_X5 (X = Li, Na, K) and $LaAlO_3$ for CO_x Selectivity

Many studies analyzed the strength of oxygen species on the catalyst surface using XPS and TPD analysis in the OCM. However, it is difficult to compare the strength of nucleophilic lattice oxygen species because of XPS. Thus, we performed CO_2-TPD analysis to compare the strength of the nucleophilic lattice oxygen species ($O_{lat(n)}$) [51]. CO_2-TPD analysis is an analytical method that analyzes the base point century of the catalyst surface by comparing the temperature at which CO_2 is desorbed. In this study, CO_2-TPD analysis was performed on prepared $LaAlO_3$_X5 (X = Li, Na, K) and $LaAlO_3$ catalysts, and the results are shown in Figure 6. Table 4 shows the temperature and amount of CO_2 desorption for the prepared catalysts. From the CO_2-TPD results, peaks displayed between about 500–700 °C mean nucleophilic lattice oxygen species ($O_{lat(n)}$) according to the studies. Therefore, we obtained that the higher temperature at which CO_2 is desorbed indicates the possession of a strong nucleophilicity of lattice oxygen by the catalysts. In the CO_2-TPD analysis results, the temperature at which CO_2 was desorbed increases in the order of $LaAlO_3$_K5, $LaAlO_3$_Na5, $LaAlO_3$_Li5, and $LaAlO_3$. These indicate that the $LaAlO_3$_K5 catalyst had a strong nucleophilicity of lattice oxygen, and the $LaAlO_3$ catalyst had a weak nucleophilicity of lattice oxygen. These results suggested that the catalysts possessing a strong nucleophilicity of lattice oxygen prefer CO_2 in CO_x and those retaining a weak nucleophilicity of lattice oxygen produce CO more easily.
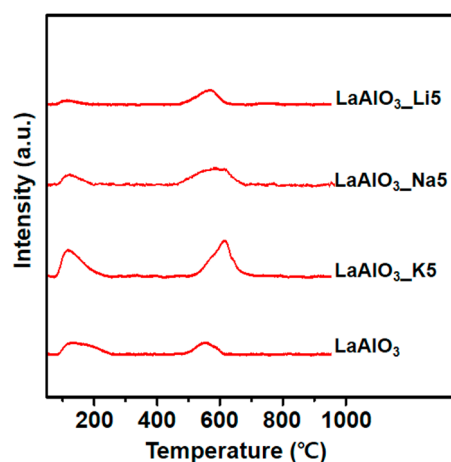
Figure 6. CO_2-TPD profile of $LaAlO_3\_X5$ (X = Li, Na, K) and $LaAlO_3$ catalysts.

Table 4. Peak areas of $LaAlO_3\_X5$ (X = Li, Na, K) and $LaAlO_3$ catalysts calculated from CO_2-TPD profiles.

	Catalyst			
	$LaAlO_3\_Li5$	**$LaAlO_3\_Na5$**	**$LaAlO_3\_K5$**	**$LaAlO_3$**
Peak (°C)	565.1	585.9	609.4	548.5
Peak area (a.u.) [a]	1563.3	1842.2	2817.9	1466.0

[a] Peak area calculated from TPD profiles with CO_2 adsorption.

4. Conclusions

In this study, we prepared alkali-added perovskite catalysts ($LaAlO_3\_XY$, X = Li, Na, K, Y = mol %) by the citrate sol-gel method for the oxidative coupling of methane (OCM). It was expected that the catalytic activity could be further enhanced by adding alkali metals since the $LaAlO_3$ perovskite catalyst has a considerable activity for the OCM reaction. As a result of conducting the OCM reaction using the prepared catalysts, we confirmed that $LaAlO_3\_XY$ had increased activity compared with the $LaAlO_3$ catalyst. We performed BET, ICP, and FE-SEM analyses to investigate the physical and chemical properties of $LaAlO_3\_X5$ catalysts. Through the analysis results of these characteristics, it was confirmed that adding alkali metals to the $LaAlO_3$ catalyst influences the characteristics of the prepared catalysts. We performed XPS and CO_2-TPD analyses to investigate the catalytic behavior of the prepared catalysts in this reaction. The XPS analysis result showed that $LaAlO_3\_XY$ catalysts with high C_2H_4 selectivity had a relatively abundant electrophilic oxygen species ($O_{lat(e)}$). The $LaAlO_3$ catalyst with a high CO_x (carbon monoxide and carbon dioxide) selectivity had a relatively abundant nucleophilic oxygen species ($O_{lat(n)}$). As a result of CO_2-TPD analysis, it was obtained that $LaAlO_3\_X5$ catalysts had a strong nucleophilicity of lattice oxygen and preferred CO_2 in CO_x. However, it was obtained that the $LaAlO_3$ catalyst had a weak nucleophilicity of lattice oxygen and produced CO more easily. These results suggested that CH_4 firstly converts methyl radicals, which are subsequently dimerized into C_2H_6 through a homogenous reaction. The nucleophilic oxygen species ($O_{lat(n)}$) on the surface of the catalysts are responsible for converting C_2H_6 (produced from the dimerization of methyl radicals) into CO or CO_2, and the electrophilic oxygen species ($O_{lat(e)}$) are responsible for converting C_2H_6 to C_2H_4. Thus, we concluded that a perovskite catalyst rich in electrophilic oxygen species should be designed to obtain an efficient OCM catalyst and that alkali-adding could be one of the efficient methods for improving catalytic activity of perovskite catalysts for the OCM reaction.

Author Contributions: Conceptualization, S.A.; syntheses, S.A. and D.K.; performance of experiments, S.A. and J.C.; writing–original draft preparation, S.A.; writing–review and editing, S.A. and J.C.J.; supervision, J.C.J.; All authors have read and agreed to the published version of the manuscript.

Conflicts of Interest: The authors declare no conflict of interest.

References

1. Guo, Z.; Liu, B.; Zhang, Q.; Deng, W.; Wang, Y.; Yang, Y. Recent advances in heterogeneous selective oxidation catalysis for sustainable chemistry. *Chem. Soc. Rev.* **2014**, *10*, 3480–3524. [CrossRef] [PubMed]
2. Farrell, B.L.; Igenegbai, V.O.; Linic, S. A viewpoint on direct methane conversion to ethane and ethylene using oxidative coupling on solid catalysts. *ACS Catal.* **2016**, *6*, 4340–4346. [CrossRef]
3. Galadima, A.; Muraza, O. Revisiting the oxidative coupling of methane to ethylene in the golden period of shale gas: A review. *J. Ind. Eng. Chem.* **2016**, *37*, 1–13. [CrossRef]
4. Lunsford, J.H. Catalytic conversion of methane to more useful chemicals and fuels: A challenge for the 21st century. *Catal. Today* **2000**, *63*, 165–174. [CrossRef]
5. Tang, P.; Zhu, Q.; Wu, Z.; Ma, D. Methane activation: The past and future. *Energy Environ. Sci.* **2014**, *7*, 2580–2591. [CrossRef]
6. Lee, J.; Yasin, M.; Park, S.; Chang, I.S.; Ha, K.S.; Lee, E.Y.; Lee, J.; Kim, C. Gas-liquid mass transfer coefficient of methane in bubble column reactor. *Korean J. Chem. Eng.* **2015**, *32*, 1060–1063. [CrossRef]
7. Sudheer, P.D.V.N.; David, Y.; Chae, C.G.; Kim, Y.J.; Baylon, M.G.; Baritugo, K.A.; Kim, T.W.; Kim, M.S.; Na, J.G.; Park, S.J. Advances in the biological treatment of coal for synthetic natural gas and chemicals. *Korean J. Chem. Eng.* **2016**, *33*, 2788–2801. [CrossRef]
8. Wood, D.A.; Nwaoha, C.; Towler, B.F. Gas-to-liquids (GTL): A review of an industry offering several routes for monetizing natural gas. *J. Nat. Gas Sci. Eng.* **2012**, *9*, 196–208. [CrossRef]
9. Nwaoha, C.; Wood, D.A. A review of the utilization and monetization of Nigeria's natural gas resources: Current realities. *J. Nat. Gas Sci. Eng.* **2014**, *18*, 412–432. [CrossRef]
10. Araujo, G.C.D.; Lima, S.; Rangel, M.D.C.; Parola, V.L.; Pena, M.A.; Fierro, J.L.G. Characterization of precursors and reactivity of $LaNi_{1-x}Co_xO_3$ for the partial oxidation of methane. *Catal. Today* **2005**, *107–108*, 906–912. [CrossRef]
11. Valderrama, G.; Boldwasser, M.R.; Navarro, C.U.D.; Tatibouët, J.M.; Barrault, J.; Batiot-Dupeyrat, C.; Maìnez, F. Dry reforming of methane over Ni perovskite type oxides. *Catal. Today* **2005**, *107–180*, 785–791. [CrossRef]
12. Perenìguez, R.; González-DelaCruz, V.M.; Holgado, J.P.; Caballero, A. Synthesis and characterization of a $LaNiO_3$ perovskite as precursor for methane reforming reactions catalysts. *Appl. Catal. B* **2010**, *93*, 346–353. [CrossRef]
13. Enger, B.C.; Lodeng, R.; Holmen, A. A review of catalytic partial oxidation of methane to synthesis gas with emphasis on reaction mechanisms over transition metal catalysts. *Appl. Catal. A* **2008**, *346*, 1–27. [CrossRef]
14. Nipan, G.D.; Artukh, V.A.; Yusupov, V.S.; Loktev, A.S.; Spesivtsev, N.A.; Dedov, A.G.; Moiseev, I.I. Effect of pressure on the phase composition of $Li(Na)/W/Mn/SiO_2$ composites and their catalytic activity for oxidative coupling of methane. *Inorg. Mater.* **2014**, *50*, 912–916. [CrossRef]
15. Colmenares, M.G.; Simon, U.; Yildiz, M.; Arndt, S.; Schomaecker, R.; Thormas, A.; Rosowski, F.; Gurlo, A.; Goerke, O. Oxidative coupling of methane on the Na2WO4-MnxOy catalyst: COK-12 as an inexpensive alternative to SBA-15. *Catal. Commun.* **2016**, *85*, 75–78. [CrossRef]
16. Wang, H.; Schmack, R.; Paul, B.; Albrecht, M.; Sokolov, S.; Rummler, S.; Kondratenko, E.V.; Kraehnert, R. Porous silicon carbide as a support for Mn/Na/W/SiC catalyst in the oxidative coupling of methane. *Appl. Catal. A* **2017**, *537*, 33–39. [CrossRef]
17. Jeon, W.; Lee, J.Y.; Lee, M.; Choi, J.W.; Ha, J.M.; Suh, D.J.; Kim, I.W. Oxidative coupling of methane to C2 hydrocarbons on theMg-Ti mixed oxide-supported catalysts at the lower reaction temperature: Role of surface oxygen atoms. *Appl. Catal. A* **2013**, *464–465*, 68–77. [CrossRef]
18. Kwon, D.; Yang, I.; Sim, Y.; Ha, J.M.; Jung, J.C. A K_2NiF_4-type $La_2Li_{0.5}Al_{0.5}O_4$ catalyst for the oxidative coupling of methane (OCM). *Catal. Commu.* **2019**, *128*, 105702. [CrossRef]
19. Sim, Y.; Kwon, D.; An, S.; Ha, J.M.; Oh, T.S.; Jung, J.C. Catalytic behavior of ABO_3 perovskites in the oxidative coupling of methane. *Mol. Catal.* **2020**, *489*, 110925. [CrossRef]
20. Nipan, G.D. Melt-assisted phase transformations of $A/W/Mn/SiO_2$ (A=Li, Na, K, Rb, Cs) composite catalysts. *Inorg. Mater.* **2017**, *53*, 553–559. [CrossRef]
21. Dedov, A.G.; Loktev, A.S.; Moiseev, I.I.; Aboukais, A.; Lamonier, J.F.; Filimonov, I.N. Oxidative coupling of methane catalyzed unexpected synergistic effect of the oxide mixtures. *Appl. Cataly. A* **2003**, *245*, 209–220. [CrossRef]
22. Driscoll, D.J.; Martir, W.; Wang, J.X.; Lunsford, J.H. Formation of gas-phase methyl radicals over magnesium oxide. *J. Am. Chem. Soc.* **1985**, *107*, 58–63. [CrossRef]

23. Arndt, S.; Laugel, G.; Levchenko, S.; Horn, R.; Baerns, M.; Scheffler, M. A Critical assessment of Li/MgO-based catalysts for the oxidative coupling of methane. *Catal. Rev.* **2011**, *53*, 424–514. [CrossRef]

24. Ghose, R.; Hwang, H.T.; Varma, A. Oxidative coupling of methane using catalysts synthesized by solution combustion method: Catalyst optimization and kinetic studies. *Appl. Catal. A* **2014**, *472*, 39–46. [CrossRef]

25. Liu, H.; Wang, X.; Yang, D.; Gao, R.; Wang, Z.; Yang, J. Scale up and stability test for oxidative coupling of methane over Na$_2$WO$_4$-Mn/SiO$_2$ catalyst in a 200 mL fixed-bed reactor. *J. Nat. Gas Chem.* **2008**, *17*, 59–63. [CrossRef]

26. Gholipour, Z.; Malekzadeh, A.; Hatami, R.; Mortazavi, Y.; Khodadadi, A. Oxidative coupling of methane over (Na$_2$WO$_4$+Mn or Ce)/SiO$_2$ catalysts: In situ measurement of electrical conductivity. *J. Nat. Gas Chem.* **2010**, *19*, 35–42. [CrossRef]

27. Rollilns, B.; Grosjean, N.; Poulston, S. The impact of the presence of various relevant gases during aging of MnNa$_2$WO$_4$/SiO$_2$ catalyst on its performance for the oxidative coupling of methane. *Appl. Catal. A* **2020**, *598*, 117606. [CrossRef]

28. Kidamorn, O.; Tiyatha, W.; Chukeaw, T.; Niamnuy, C.; Chareonpanich, M.; Sohn, H.; Seubsai, A. Synthesis of value-added chemicals via oxidative coupling of methanes over Na$_2$WO$_4$-TiO$_2$-MnO$_x$/SiO$_2$ catalysts with alkali or alkali earth oxide additives. *ACS Omega* **2020**, *5*, 13612–13620. [CrossRef]

29. Arndt, S.; Otremba, T.; Simon, U.; Yildiz, M.; Schubert, H.; Schomacker, R. Mn-Na$_2$WO$_4$/SiO$_2$ as catalyst for the oxidative coupling of methane. What is really known? *Appl. Catal. A* **2012**, *425–426*, 53–61. [CrossRef]

30. Nibbelke, R.H.; Scheerova, J.; Decroon, M.H.J.M.; Maring, G.B. The oxidative coupling of methane over MgO-based catalysts: A steady-state isotope transient kinetic analysis. *J. Catal.* **1995**, *156*, 106–119. [CrossRef]

31. Luo, L.; You, R.; Liu, Y.; Yang, J.; Zhu, Y.; Wen, W.; Pan, Y.; Qi, F.; Huang, W. Gas-phase reaction network of Li/MgO-catalyzed oxidative coupling of methane and oxidative dehydrogenation of ethane. *ACS Catal.* **2019**, *9*, 2514–2520. [CrossRef]

32. Qian, K.; You, R.; Guan, Y.; Wen, W.; Tian, Y.; Pan, Y.; Huang, W. Single-site catalysis of Li-MgO catalysts for oxidative coupling of methane reaction. *ACS Catal.* **2020**, *10*, 15142–15148. [CrossRef]

33. Tang, L.G.; Yamaguchi, D.; Wong, L.; Burke, N.; Chiang, K. The promoting effect of ceria on Li/MgO catalysts for the oxidative coupling of methane. *Catal. Today* **2011**, *178*, 172–180. [CrossRef]

34. Gu, S.; Oh, H.S.; Choi, J.W.; Suh, D.J.; Jae, J.; Choi, J.; Ha, J.M. Effects of metal or metal oxide additives on oxidative coupling of methane using Na$_2$WO$_4$/SiO$_2$ catalysts: Reducibility of metal additives to manipulate the catalytic activity. *Appl. Catal. A* **2018**, *562*, 114–119. [CrossRef]

35. Choudhary, V.R.; Rane, V.H.; Pandit, M.Y. Comparison of alkali metal promoted MgO catalysts for their surface acidity/basicity and catalytic activity/selectivity in the oxidative coupling of methane. *J. Chem. Tech. Biotechnol.* **1997**, *68*, 177–186. [CrossRef]

36. Elkins, T.W.; Roberts, S.J.; Hagelin-Weaver, H.E. Effects of alkali and alkaline-earth metal dopants on magnesium oxide supported rare-earth oxide catalysts in the oxidative coupling of methane. *Appl. Catal. A* **2016**, *528*, 175–190. [CrossRef]

37. Miro, E.; Santamaria, J.; Wolf, E.E. Oxidative coupling of methane on alkali metal-promoted nickel titanate: I. Catalyst characterization and transient studies. *J. Catal.* **1990**, *124*, 451–464. [CrossRef]

38. Rane, V.H.; Chaudhari, S.T.; Choudhary, V.R. Influence of alkali metal doping on surface properties and catalytic activity/selectivity of CaO catalysts in oxidative coupling of methane. *J. Nat. Gas Chem.* **2008**, *17*, 313–320. [CrossRef]

39. Ito, T.; Wang, J.; Lin, C.H.; Lunsford, J.H. Oxidative dimerization of methane over a lithium-promoted magnesium oxide catalyst. *J. Am. Chem. Soc.* **1985**, *107*, 5062–5068. [CrossRef]

40. Kim, I.; Lee, G.; Na, H.B.; Ha, J.M.; Jung, J.C. Selective oxygen species for the oxidative coupling of methane. *Mol. Catal.* **2017**, *435*, 13–23. [CrossRef]

41. Sim, Y.; Kwon, D.; Ha, J.M.; Jung, J.C. Preparation of LaAlO$_3$ perovskite catalysts by simple solid-state method for oxidative coupling of methane. *Catal. Today* **2020**, *352*, 134–139. [CrossRef]

42. Berger, T.; Schuh, J.; Sterrer, M.; Diwald, O.; KnÖzinger, E. Lithium ion induced surface reactivity changes on MgO nanoparticles. *J. Catal.* **2007**, *247*, 61–67. [CrossRef]

43. Zhang, Y.; Huang, Y.; Wang, X.; Sun, J.; Si, R.; Zhou, H. Collective and individual impacts of the cascade doping of alkali cations in perovskite single crystals. *J. Mater. Chem. C* **2020**, *43*, 15350–15360. [CrossRef]

44. Kiani, D.; Sourav, S.; Baltrusaitis, J.; Wachs, I.E. Oxidative coupling of methane (OCM) by SiO2-supported tungsten oxide catalysts promoted with Mn and Na. *ACS Catal.* **2019**, *9*, 5912–5928. [CrossRef]

45. Zhang, H.B.; Lin, G.D.; Wan, H.L.; Liu, Y.D.; Weng, W.Z.; Cai, J.X.; Shen, Y.F.; Tsai, K.R. Active-oxygen species on non-reducible rare-earth-oxide-based catalysts in oxidative coupling of methane. *Catal. Lett.* **2001**, *73*, 141–147. [CrossRef]

46. Lunsford, J.H. The catalytic oxidative coupling of methane. *Angew. Chem. Int. Ed. Engl.* **1995**, *34*, 970–980. [CrossRef]

47. Wang, H.; Cong, Y.; Yang, W. Oxidative coupling of methane in Ba0.5Sr0.5Co0.8Fe0.2O3- tubular membrane reactors. *Catal. Today* **2005**, *104*, 160–167. [CrossRef]

48. He, Y.; Yang, B.; Cheng, G. On the oxidative coupling of methane with carbon dioxide over CeO$_2$/ZnO nanocatalysts. *Catal. Today* **2004**, *98*, 595–600. [CrossRef]

49. Lee, M.R.; Park, M.J.; Jeon, W.; Choi, J.W.; Suh, Y.W.; Suh, D.J. A kinetic model for the oxidative coupling of methane over Na$_2$WO$_4$/Mn/SiO$_2$. *Fuel Process. Technol.* **2012**, *96*, 175–182. [CrossRef]

50. Yoon, S.; Lim, S.; Choi, J.W.; Suh, D.J.; Song, K.H.; Ha, J.M. Study on the unsteady state oxidative coupling of methane: Effects of oxygen species from O$_2$, surface lattice oxygen, and CO$_2$ on the C$_2$ selectivity. *RSC Adv.* **2020**, *10*, 35889. [CrossRef]

51. Gambo, Y.; Jalil, A.A.; Triwahyono, S.; Abdulrasheed, A.A. Recent advances and future prospect in catalysts for oxidative coupling of methane to ethylene: A review. *J. Ind. Eng. Chem.* **2018**, *59*, 218–229. [CrossRef]